Removal of phenol and chlorine from wastewater using steam activated biomass soot and tire carbon black

Anna Trubetskaya[a,*], Jens Kling[b], Olov Ershag[c], Thomas Attard[d],
Elisabeth Schröder[e]

[a]*Mechanical Engineering Department, National University of Ireland, H91TK33 Galway, Ireland*
[b]*Center for Electron Nanoscopy, Technical University of Denmark, 2800 Kgs. Lyngby, Denmark*
[c]*Scandinavian Enviro Systems AB, Regnbågsgatan 8C, 41755, Göteborg, Sweden*
[d]*Department of Chemistry, The University of York, Heslington, York, YO10 5DD, UK*
[e]*IKET, Karlsruhe Institute of Technology, 76344, Eggenstein-Leopoldshafen, Germany*

Abstract

This study aims to demonstrate a novel method for removing toxic chemicals using soot produced from wood and herbaceous biomass pyrolyzed in a drop tube reactor and tire pyrolytic carbon black. The influence of ash content, nanostructure, particle size, and porosity on the filter efficiency of steam activated carbon materials was studied. It has been shown for the first time that steam activated soot and carbon black can remove phenol and chloride with the filter efficiencies as high as 95%. The correlation of the filter efficiency to material properties showed that the presence of alkali and steam activation time were the key parameters affecting filter efficiencies. This study shows that steam activated biomass soot and tire carbon black are promising alternatives for the wastewater cleaning.

Keywords: wastewater filters, biomass soot, tire carbon black, H_2O

*Corresponding author. anna.trubetskaya@nuigalway.ie

activation, pyrolysis

1. Introduction

Clean water is an essential resource for human life and surrounding ecosystem. Population growth and climate change had a large impact on fresh water scarcity [1]. Recovery and recycling technology of wastewater has become a growing trend in the past decades to achieve water sustainability. Polycyclic aromatic hydrocarbons (PAH) and phenols are considered to be priority organic pollutants since they can harm humans and aquatic life at low concentrations [2–5]. Safe drinking water is vital for human consumption and thus, requires disinfection using chlorine that can react with the organic matter to form toxic products [6, 7]. The limits of phenol ($2\,\mathrm{mg\ l^{-1}}$) and chlorine ($2\,\mathrm{mg\ l^{-1}}$) in drinking water [8, 9] and less than $0.5\,\mathrm{mg\ l^{-1}}$ of phenol and $0.2\,\mathrm{mg\ l^{-1}}$ in industrial wastewater are acceptable [10].

The removal of phenol and chlorine from drinking water and wastewater is of great importance. A number of methods *i.e.* coagulation, filtration, precipitation, etc. have been used for the removal of organic pollutants and chlorine from polluted drinking water and wastewater [2, 11–15]. Filtration using solid activated sorbents is the most efficient method for the removal of organic contaminants and chlorine in drinking water and wastewater [16–19]. The most important properties of carbonaceous materials for the removal of organic pollutants and chlorine are high packing density, high micropore volume and low ash content [20]. In the previous studies, the activated carbon, carbon nanotubes and nanofibers (CNFs), industrial fly ash and biochar were used as alternative sorbents to remove toxic chemicals from the wastew-

2

ater [21–24]. The activated carbons are characterized by a large specific surface area, well-developed porosity and tunable surface-containing functional groups. However, commercial activated carbons are very costly [2]. Locally available carbon materials such as biomass, agricultural and industrial wastes can be used as low-cost and environmentally friendly sorbents [25]. Soot with the fullerene onion-ring structure is a more effective sorbent of organic impurities in aqueous phase than traditional activated carbons because soot has low ash content and small pore size [26]. In recent years, the disposal of waste tires has become an important issue. The liquid hydrocarbons and solid char residue from thermal conversion of waste tires have potential to be used as environmentally benign fuel and activated carbon [27]. The post-carbonization of steam activated tire carbon black resulted in an excellent adsorption capacity for the removal of phenol and trace oils from wastewater [28]. Pyrolytic carbon black possesses relatively high adsorption capacity for aqueous species of large molecular weight [29]. In addition, pyrolytic carbon black exhibited greater adsorption capacity for acetone ($\approx 67\,\%$) in gas cleaning applications compared to other commercial active carbons [20]. Previous studies showed that activated carbon from corncobs and palm seed coat can be produced in one-step using a physical activation method in steam or carbon dioxide [30, 31]. The corncobs char was steam activated at 850°C for 1 h, whereas the palm seed coat was initially carbonized with dolomite at 500°C for 3 h, washed with HCl and water to remove contaminations, dried at 110°C and activated in a carbon dioxide at 850-900°C for 30 min. The results of fullerene steam activation indicated that the heat treatment temperature and time are the dominating parameters to control the development

3

of porosity and specific surface area [32, 33]. Similarly, both steam and CO_2 activation of pyrolytic tire carbon black increased the surface area from $60\,\mathrm{m}^2$ g^{-1} to the range of $272\text{-}1118\,\mathrm{m}^2\,\mathrm{g}^{-1}$ [28, 34]. Similar sizes of specific surface area of the pyrolytic tire carbon black were obtained for the same conversion for both activation media, however, the steam activation was two or three times faster than CO_2 activation [35, 36].

High soot formation is a major technical challenge in the entrained flow biomass gasification. Soot yields obtained in CO_2 gasification of biomass vary from 4 to $16\,\mathrm{wt.}\%$ and depend mainly on the feedstock composition and heat treatment temperature [37, 38]. In order to improve the economic performance and reliability of entrained flow gasification, biomass soot has the potential to be captured, activated and further used as an sorbent to remove a broad range of pollutants from wastewater. The renewable biomass soot-based sorbents as the waste products of gasification have a clear environmental advantage over coal-based carbons in filtering technology. To address this knowledge gap, soot from wood and herbaceous biomass was produced in a drop tube reactor at $1250°\mathrm{C}$. The pyrolytic tire carbon black and soot were steam activated, and then thoroughly investigated for the removal of phenol and chlorine from aqueous solutions. The use of steam activated biomass soot and tire carbon black has not been previously investigated. There, the specific objectives of this study were to: (1) to investigate the filtration performance of activated biomass soot and pyrolytic tire carbon black and (2) to correlate the material properties to the filtration performance. The results of this study provide a clear basis for understanding the steam activation effects on the design and operation of activated soot-based filters.

4

2. Materials and methods

2.1. Soot and tire carbon black characterization

Elemental analysis. The elemental analysis of samples was performed on Elemental Analyser 2400 CHNS/O Series II (Perkin Elmer, USA). Acetanilide was used as a reference standard. The ash content was determined using a standard ash test at 550°C, according to the procedure described in DIN EN 14775.

Proximate analysis. The moisture and volatile content of samples was performed according to the procedures described in DIN EN 14774-1 and DIN EN 51720.

Ash compositional analysis. Prior to ICP analysis, samples were pre-heated in oxygen at 5°C min^{-1} up to 550°C and kept at that temperature for 7 h. The ash sample was dissolved in ultrapure water at 120°C for 1 h, and then the solution was filtered and analyzed by ICP-OES/IC, according to procedures described in DIN EN 51719 and DIN EN 15289.

Transmission electron microscopy. Soot nanostructure and particle size were studied using a FEI Titan transmission electron microscope operated at 120 keV. The particle size of soot samples was estimated manually from TEM images using the ImageJ software [39, 40]. Only clearly visible primary particles were selected for accurate analysis. The data were assessed to establish particle size distributions. For size analysis, soot particles were assumed spherical. Particle size analysis was conducted on 200 particles at each operating condition. The length of graphene layers, separation distance

5

between layers and curvature of soot and tire carbon black samples were characterized using TEM. Standard deviation was calculated for curvature, fiber length (see definition below) and separation distance of graphene layers as described in the supplementary material (equation 1). The curvature of a single graphene sheet was calculated as shown in the supplementary material (equation 2).

N_2 *physisorption analysis.* The specific surface area (SSA) of biomass soot was determined based on N_2 physisorption (77 K). The samples were degassed at 350°C for 42 h. The surface area was determined by Brunauer-Emmett-Teller (BET) by Nova 4000e (Quantachrome, Germany) instrument. The micro and mesopore size distributions were determined by Density Functional Theory (DFT) method under the assumption of a slit-shaped pore [41]. The pores were classified into three types: macropores ($\geq$ 50 nm), mesopores (2-50 nm), and micropores ($\leq$ 2 nm) [42]. Porosity (ϕ) was estimated in equation 1:

$$\phi = \frac{V_{cum}}{V_{cum} + V} \tag{1}$$

In equation 1, V_{cum} is the total cumulative pore volume (cm^3 g^{-1}). V is the specific volume that was calculated under the assumption of density of carbon black (2.246 g cm^{-3}) [43].

2.2. Fast pyrolysis in drop tube furnace

Wood and herbaceous biomass were reacted in the drop tube furnace (DTF) at 1250°C. The high heating rate and short residence times obtained with the drop tube furnace simulate the conditions in entrained-flow gasifiers. Based on previous work [44], operation at 1250°C was selected to maximize

6

the soot yield. The reactor consists of an alumina tube (internal diameter: 54 mm, heated length: 1.06 m) heated by four heating elements with independent temperature control, as shown in Figure 1.
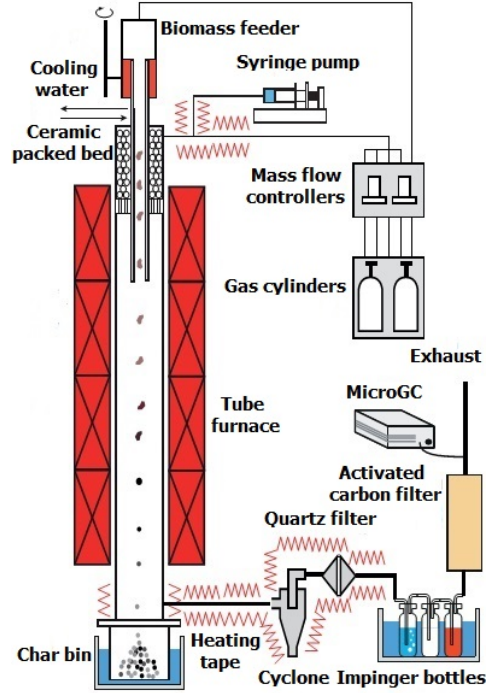

Figure 1: Schematic view of the drop tube reactor.

Gas flow rate into the reactor is regulated by mass flow controllers (EL-FLOW® Select, Bronkhorst High-Tech B.V.). The feeding system is based on a syringe pump that displaces a bed of fuel that falls directly into the high temperature zone in the reactor through a water-cooled probe. The syringe pump was vibrated to ensure stable feeding of the fuel particles. In each experiments, ≈ 5 g of biomass were fed to the reactor at a rate of 0.2 g min^{-1}. Both primary (0.18 l min^{-1} measured at 20°C and 101.3 kPa) and

secondary ($4.8\,l\,min^{-1}$ measured at 20°C and 101.3 kPa) feed gases were N_2. The residence time of fuel particles was estimated to be about 1 s, taking into account density changes during pyrolysis. Reaction products were separated into coarse particles (mainly char and fly ashes), fine particles (mainly soot and ash aerosols), permanent gases, and tars. Course particles were captured in a cyclone (cut size 2.5μm). Soot particles exited the cyclone and were collected on a grade QM-A quartz filter with a diameter of 50 mm (Whatman, GE Healthcare Life Science). Soxhlet extraction using acetone as the solvent was performed on soot samples from pyrolysis of wood and herbaceous biomass by extracting 0.1 g of the solid placed within a 100 ml Soxhlet apparatus for 12 h.

2.3. Steam activation

The steam activation experiments were performed in a tubular reactor that can be operated up to 1100°C, as reported by Schröder et al. [45]. The tubular reactor consists of a high-temperature resistant stainless steel tube (1), which is located in a tubular, electrically heated furnace, as shown in Figure 2. The steel tube is equipped with a removable inner tube (2) made of the same material. Gas supply is attached to the inner tube and at its lower end a small, removable case (40 mm inner diameter, 70 mm length) is fixed. The bottom of this case is porous which allows sufficient flow perfusion. The soot samples were placed onto the porous bottom of the case prior to the experiment by taking the inner tube out of the furnace. After replacing the inner tube into the preheated furnace, the sample was purged with nitrogen. Once the activation temperature of 900°C was reached, the gas flow was switched from N_2 to steam with a flow rate of 150-300 ml min^{-1},

8

which was produced by a steam generator (HG2000-4, TWD Dampftechnis-che Produkte). The activation was terminated by switching the steam flow to nitrogen flow. Then the inner tube was removed from the furnace and cooled to room temperature while the N_2 flow was maintained to avoid oxidation of the carbon material.
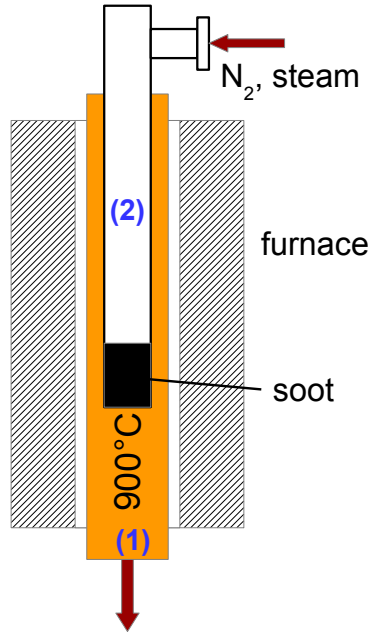

Figure 2: Schematic view of the tubular reactor for soot and carbon black activation at KIT, IKET.

The sample mass was measured prior to and after the activation experiments to determine the conversion that is defined in equation 2 [45]:

$$X_{sf} = \left(1 - \frac{m}{m_0}\right) \cdot 100 \tag{2}$$

In equation 2, m_0 and m are the initial sample mass and actual sample mass.

The BET and pore size of non-treated and activated carbon samples were determined.

2.4. Filtration

The vacuum filtration was performed on 10 mm diameter glass Büchner microfunnel P4 (Witeg, Germany), as shown in the supplemental material (Figure S-2). Prior to filtration, phenol and chlorine were dissolved at once in deionized water and stirred for 30 min. 125 ml of water containing phenol and chlorine was passed through the 5 mm-deep densely packed activated carbon bed. Two stainless steel mesh circular-cutten pieces (316L, TWP Inc., mesh width of 42 μm) were placed at the top and at the bottom of a carbon bed to hold soot or pyrolytic tire carbon black particles. The filtration experiments were repeated two times.

2.5. Analysis of filtrate

The collected aqueous filtrate was analyzed to determine the concentrations of remaining phenol and chlorine in the water. The solution of phenol and chlorine mixtures of different concentrations (1, 2 and 3 mg l^{-1}) was prepared. The analysis of phenolic compounds and chlorine were performed at Eurofins Germany.

Prior to GC analysis, phenolic compounds were converted to acetates by the addition of acetic anhydride and subsequently extracted with n-hexane [46]. The phenolic compounds were annotated using a dual detector system GC-MS 5975C TAD Series / GC-FID 7890A (Agilent Technologies, USA) and ZB5MS capillary column (30 m length, 0.25 mm internal diameter, 0.25 μm film thickness) in accordance with DIN EN 12673 standard.

10

The injection volume was $2\,\mu$l. Samples were automatically injected using the splitless-injection mode. The temperatures of the injector and transfer line of the GC to the MS were kept at 250°C and 270°C, respectively. The column temperature program ran from 120 to 260°C. After holding the oven temperature at 120°C for the first 1 min the temperature was increased to 230°C at a rate of 15°C min^{-1}, then to 260°C at a rate of 30°C min^{-1}, and hold for 8 min. Helium was used as a carrier gas with a constant flow rate of 1 ml min^{-1}. The mass spectrometer with a quadrapolar type analyzer scanned the range from m/z 50 to m/z 550 for the qualitative determinations and it was operated in selected ion-monitoring (SIM) mode during the quantitative analysis. The mass spectrometer was operated at unit mass resolution. A solvent delay time of 3.5 min was used to protect the ion multiplier of the MS instrument from saturation. For the semiquantification of annotated chlorophenols and alkylphenols, the external standards (13172-ME5 and 13147-ME5, NEOCHEMA Germany) were used. The internal standards (2,4,6-tribromophenol and 2,4-dibromophenol) were added in an aliquot of the concentrated extract to quantify the non-reacted phenol in the wastewater.

The quantification of chlorine in deionized water was performed on an ion chromatograph IC 930 Compact Flex (Metrohm AG, Switzerland) with Metrosep A Supp 5 anion column (4x150 mm, $5\,\mu$m particle size) that was safeguarded with Metrosep A Supp 4/5 Guard precolumn in accordance with DIN EN 10304-1 standard. The mobile phase (Na_2CO_3: 3.2 mmol l^{-1} and $NaHCO_3$: 1 mmol l^{-1}) was degassed and filtered. The injection volume was $10\,\mu$l. The flow rate of the mobile phase was set at 0.8 ml min^{-1}. Water

11

was used as a diluent. Data acquisition and processing were performed using MagicNet 3.2 (Metrohm AG, Switzerland).

3. Results

3.1. Feedstock characterization

The Scots pinewood (Pinus sylvestris L.) and beechwood (Fagus sylvatica) were harvested in Jylland (Denmark) and Hannover (Germany). Both heartwood and early wood were used in the present study. The wheat straw (Triticum aestivum L.) originates from Denmark (Aabenraa plantage). The fuels were milled on a Retsch rotor mill RZ200 and sieved to particle size fractions of 0.05-0.2 mm and further reacted in a drop tube reactor. Pyrolytic tire carbon black was supplied by Scandinavian Enviro Systems AB. The ultimate and proximate analysis of the soot and pyrolytic carbon black was carried out at Eurofins Freiberg. The results are shown in Table 1. The iodine adsorption number of the pyrolytic tire carbon black was in the range 83-102 mg kg^{-1}. The ash composition was calculated on the dry basis.

Table 1: Proximate, ultimate and ash analyses of biomass soot and pyrolytic tire carbon black. The proximate and ultimate analysis is based on the ash containing soot and tire carbon black (wt.% on dry basis).

Fuel	Pinewood soot	Beechwood soot	Wheat straw soot	Pyrolytic tire carbon black
Proximate and ultimate analysis, (wt.% on dry basis)				
Moisture (as received)	0.1	0.1	0.1	0.3
Ash ($550\,^{\circ}$C)	0.3	3	6	21
C	99	96.4	87.3	70
H	0.4	0.4	0.6	0.6
O	0.3	0.2	5.5	5.3
N	n.d.	n.d.	n.d.	0.3
S	<0.01	<0.01	0.6	2.8
Cl	<0.01	<0.01	0.5	0.08
Ash compositional analysis, (mg kg^{-1} tires/biomass on dry basis)				
Al	n.d.	n.d.	n.d.	2000
Ca	1200	7100	8300	9500
Fe	n.d.	n.d.	n.d.	8500
K	650	10600	11400	1600
Mg	n.d.	n.d.	n.d.	1100
Na	50	2000	1200	2300
P	n.d.	n.d.	n.d.	100
Si	300	2500	28300	51000
Ti	n.d.	n.d.	n.d.	300
Zn	n.d.	n.d.	n.d.	20000
Soot and tire carbon black after steam activation, wt. % (g g^{-1} soot/tire carbon black)				
Ash ($550\,^{\circ}$C)	0.4	3.5	7.1	25.2

3.2. Soot and tire carbon black steam activation

Figure 3(a) shows the BET surface area as a function of tire carbon black and soot conversion resulting from the steam activation. The specific surface areas of soot and tire carbon black increased with the increase of carbon conversion using equation 2. The pinewood soot and tire carbon black

13

reached a maximum conversion of 70 %, resulting in a specific surface area decrease due to the lack of carbon. The steam activation of soot, particularly beechwood and wheat straw soot samples, was mainly kinetically controlled, and to a minor extent controlled by the external diffusion, as shown in the supplementary material (Table S-1).
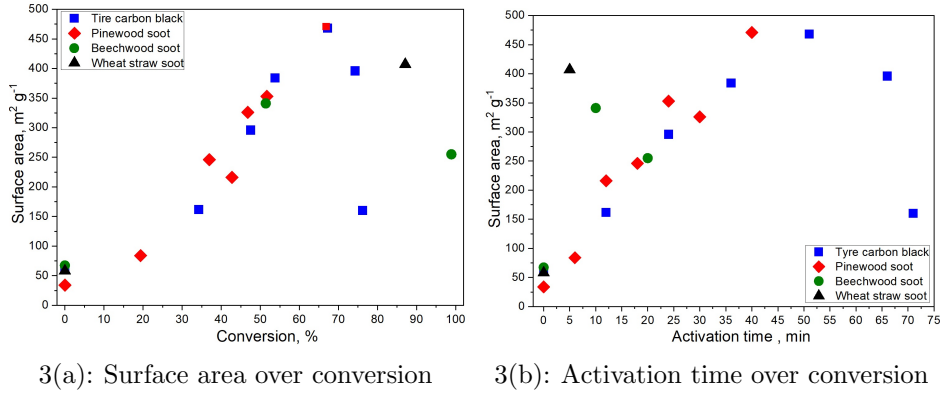

3(a): Surface area over conversion   3(b): Activation time over conversion

Figure 3: (a) Surface area over conversion and (b) Activation time (min) over conversion of tire carbon black and pinewood, beechwood and wheat straw soot in the tubular reactor using steam at 900°C.

The results showed that pinewood soot and tire carbon black required the activation time to be in the range of 40-50 min to obtain the highest specific surface area of $470 \, \mathrm{m^2 \ g^{-1}}$, as shown in Figure 3(b). The 5-20 min steam activation of beechwood and wheat straw soot led to the higher specific surface areas (260 and $400 \, \mathrm{m^2 \ g^{-1}}$) at about 90 % carbon conversion compared to the activation of pinewood soot and tire carbon black at lower conversion rates. The residence time for the tire carbon black and soot activation varied due to the differences in sample properties (bed height, particle size) and steam flow which influence the heat and mass transfer in the tubular reactor.

14

In the present work, the residence time was a less explicit descriptor for the characterization of soot activation than the conversion due to the coupling of surface formation with the carbon reaction.

Table 2 summarizes the pore characteristics of non-treated and activated tire carbon black, pinewood and beechwood soot with regards to the size of micro- and mesopore and total porosity.

Table 2: Pore size analysis and porosity of tire carbon black, pinewood, and beechwood soot samples, determined by Density Functional Theory (DFT) method using N_2 physisorption data.

| Sample	Activation	Cumulative pore volume	Mean pore diameter		Porosity
			Micropore	Mesopore	
	min	$cm^3 \ g^{-1}$	nm		%
Tire carbon black	0	0.4		19.2	47.4
	10	0.4	1.6	20.1	47.6
	65	0.6	1.5	19.2	55.1
Pinewood soot	0	0.3	1.5	17.5	41.1
	10	0.7	1.5	17.5	61.8
	30	1.3	1.5	12.2	73.7
Beechwood soot	0	0.4	1.5	19.2	44.3
	10	0.5	1.5	17.5	53.8

The porosity of all carbon samples increased during steam activation. The pinewood soot attained a higher porosity (73.7 %) than the beechwood soot (53.8 %) and tire carbon black (55.1 %) at maximal conversion of steam activation, as shown in the supplementary material (Figures S-4 and S-5). The porosities of non-treated and activated tire carbon black and beechwood soot changed only slightly, while the porosity of pinewood soot increased significantly more from 41.1 to 73.7 % in comparison to other soot samples.

The non-treated pinewood and beechwood soot exhibited type I adsorption isotherms, indicating that these samples contain a large fraction of micropores, as shown in the supplementary material (Figure S-4)[42]. The non-treated carbon black showed also type I adsorption isotherm, but probably contained less micropores than soot particles. The long steam activation of the pinewood soot led to the increased formation of both micro- and mesopores following the type II adsorption isotherm. The activated beechwood soot and tire carbon black possessed the type I adsorption isotherm, indicating the increased microporosity with the presence of few mesopores.

The micropore mean diameter of all samples remained unchanged during steam activation. This is probably due to the detection limits of micropore size with N_2 physisorption. The mesopore mean diameter of activated pinewood soot at maximal conversion decreased from 17.5 to 12.2 nm, whereas a mesopore volume increased from 0.39 to 1.25 cm^3 g^{-1}, probably due to the increased number of pores[47]. The mesopore size of beechwood soot and tire carbon black decreased only slightly during steam activation. This indicates a major influence of carbon origin on the pore formation and characteristics.

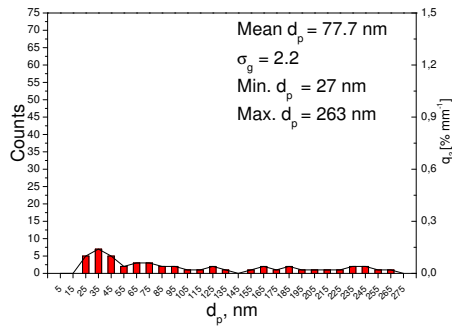### 3.3. Particle size and nanostructure analysis

The size distribution of the tire carbon black and primary soot particles was plotted as a fraction of the number of particles in each size range as shown in Figure 4.
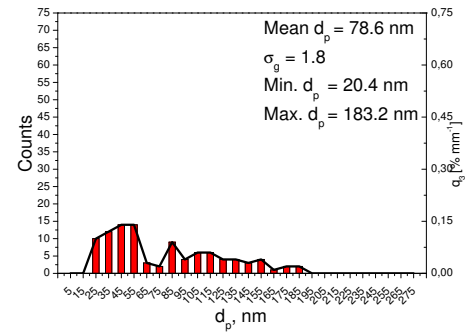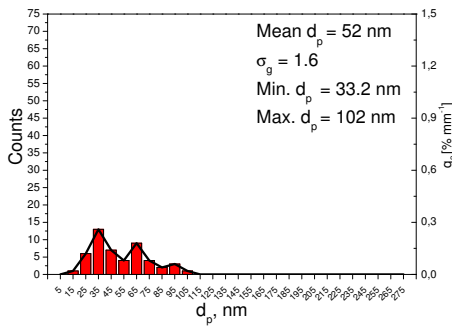
16
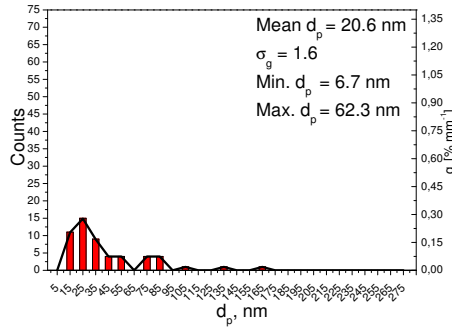
4(a): Tire carbon black
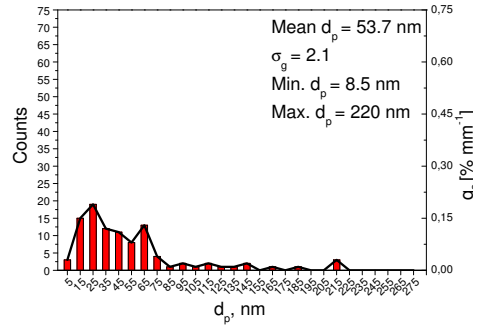
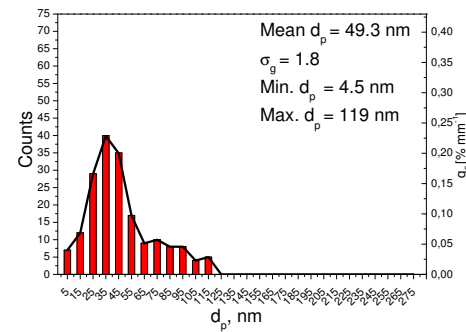4(b): Activated tire carbon black
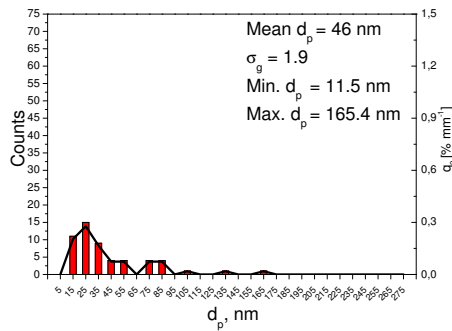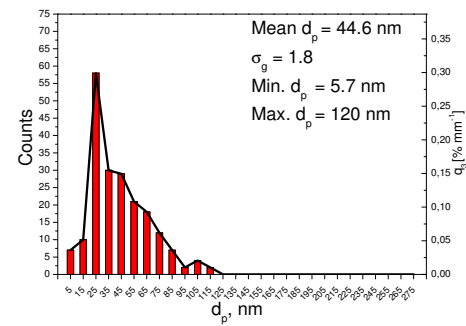
4(c): Pinewood soot

4(d): Activated pinewood soot

4(e): Beechwood soot

4(f): Activated beechwood soot

4(g): Wheat straw soot

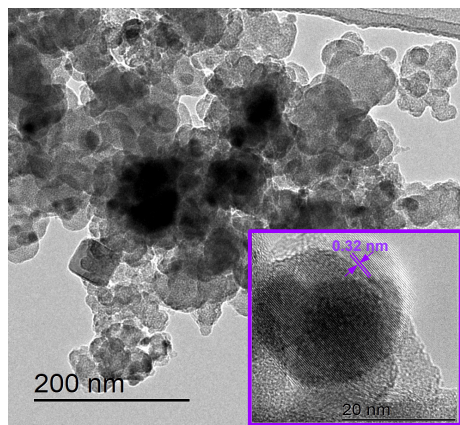4(h): Activated wheat straw soot

17

Figure 4: Particle size distributions of non-treated and steam activated (5-10 min) tire carbon black, pinewood, beechwood and wheat straw soot samples.

The calculated geometric mean diameters of non-treated and steam activated samples varied from 20.6 to 78.6 nm, and were similar to the values reported for biomass smoke (30-50 nm) in other studies [48, 49]. The differences in particle size of non-treated and activated samples were small, except for the tire carbon black. The geometric mean particle diameter of activated carbon black increased from 20.6 to 53.7 nm, as shown in Figures 4(a)-4(b). This indicates that feedstock has a strong influence on the observed differences in particle size during steam activation.

No large differences in the particle clustering were determined among non-treated and activated tire carbon black and soot, as shown in Figure 5(a)-5(b) and previous studies [44]. TEM images of non-treated tire carbon black showed clustering of individual particles without clearly defined boundaries. The particle size of non-treated tire carbon black was difficult to determine due to the mixture of spherical and irregular-shaped particles.

The nanostructure of the non-treated and activated tire carbon black and soot was studied by TEM, as shown in Figures 5-6. The soot particles appeared as agglomerates. All primary tire carbon black and soot particles exhibited a core-shell structure, with both single and multiple cores, confirming the previous results of Trubetskaya et al. [38]. The primary particles in wheat straw soot consisted of mostly single core particles with a large core, whereas pinewood soot and tire carbon black contained mostly multiple core particles. The primary particles in beechwood soot possessed a mixture of single and multiple core structures. Compared to the cores of pinewood soot and tire carbon black, the multiple cores of beechwood soot particles were located closer to each other due to particle coalescence at an earlier stage of
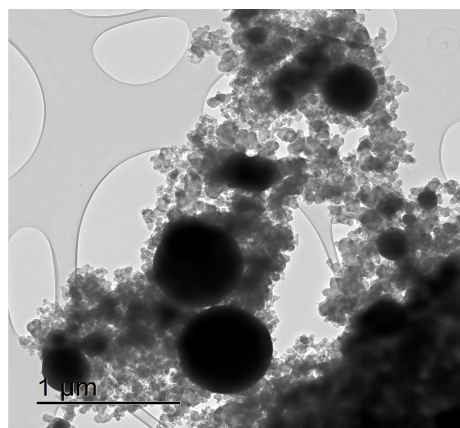
18

the particle formation. Liati et al.[50] related the multiple structure to an early phase of soot formation by nuclei coalescence and further development as a single particle.
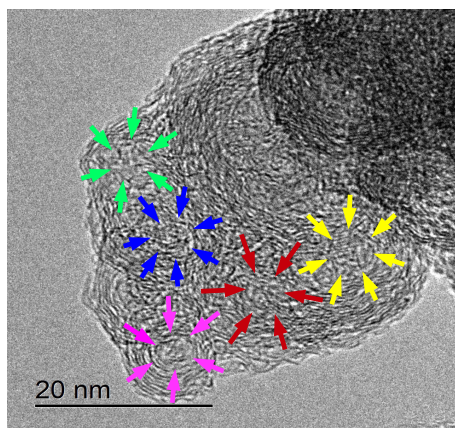

5(a): Tire carbon black
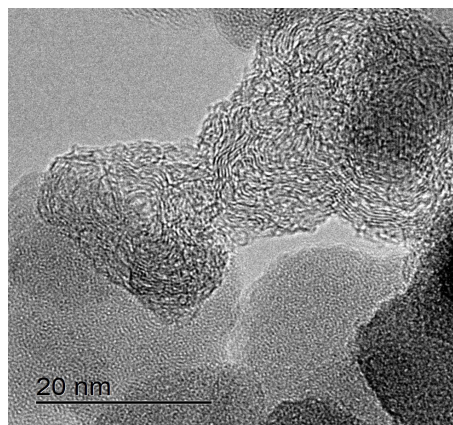
5(b): Tire carbon black

5(c): Activated tire carbon black

5(d): Activated tire carbon black

Figure 5: TEM images of non-treated and steam activated (5 min) tire carbon black. The purple rectangle indicates the sulfur crystals over the tire carbon black surface.
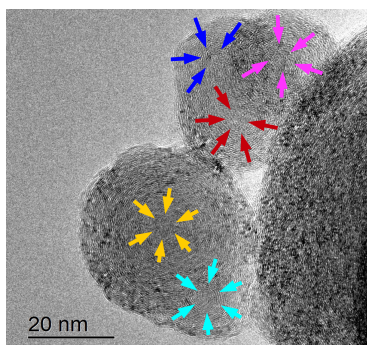
6(a): Pinewood soot
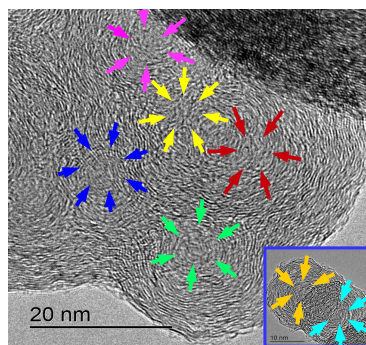
6(b): Activated pinewood soot
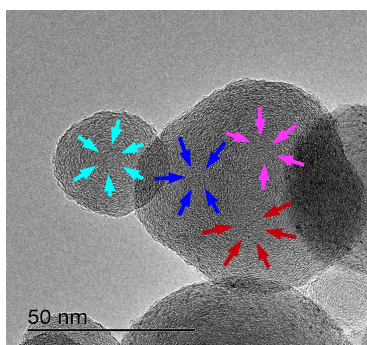
6(c): Beechwood soot
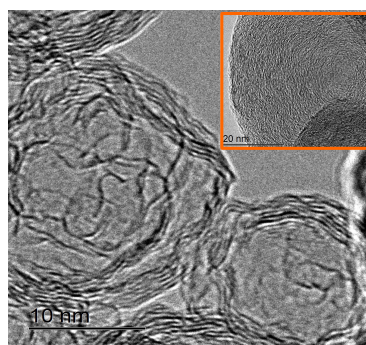
6(d): Activated beechwood soot
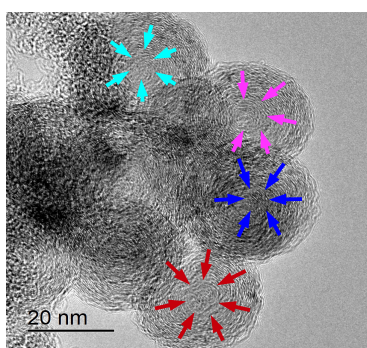
6(e): Wheat straw soot
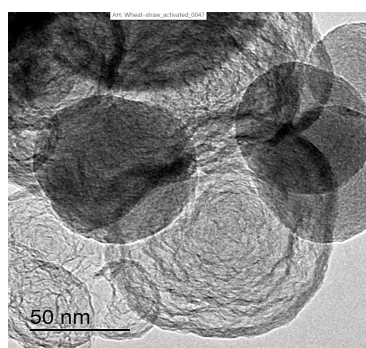
6(f): Activated wheat straw soot

Figure 6: TEM images of non-treated and steam activated (5-10 min) pinewood, beechwood and wheat straw soot samples. The blue rectangle shows multiple cores which are located very closely. The orange rectangle indicates a different type of soot particle.

20

The multiple core structure of pinewood soot and tire carbon black reflects formation by coalescence of several smaller particles, with this process governed by the particle concentration [51]. Both fine and large primary soot and tire carbon black particles consisted of graphene sheets, which grow circumferentially from the particle core. The nanostructure that is closer to the outer surface of smaller and larger particles seems to be similar as shown in Figures 5-6. All soot samples exhibited a well-ordered graphitic structure, whereas the tire carbon black showed two different carbon structures. The straight graphene layers of the neighboring particles appear to be merged, forming a continuous surface over a large number of crystallites, as shown in Figure 5(a). Another type of carbon structure with more curved and less elongated graphene layers was found in the non-treated tire carbon black which disappeared with steam activation, as shown in Figure 5(b). In addition, the sulfur crystals with a separation distance of 0.32 nm were detected over the carbon structure of non-treated and activated tire carbon black [52], as shown in Figure 5(a).

Table 3 summarizes the characteristics of different soot samples with regards to single or/and multiple cores, curvature and separation distance of graphene layers. The graphene segments of the non-treated tire carbon black and soot were well ordered and flat with the smaller curvature of an average particle size (0.85-0.88; flat graphene $\approx$1 [53]). However, the graphene segments of the activated tire carbon black and soot were slightly less ordered. The mean separation distance of activated tire carbon black and soot graphene segments (0.33-0.34 nm) was similar to that that of graphite (0.335 nm), indicating the high degree of crystallinity [50]. The mean sep-

aration distance of activated beechwood and wheat straw soot decreased slightly, indicating a further decrease in oxygenated groups during steam activation [54]. The length of graphene segments was also similar to graphite and remained unchanged after steam activation.

Table 3: Summary of tire carbon black and pinewood, beechwood, and wheat straw soot characteristics (cure, curvature, separation distance).

Sample	Non-treated				Activated			
	Fiber length	Curvature[2]	d_{sep}[1,2]	Core[3,4]	Fiber length	Curvature[2]	d_{sep}[1,2]	Core[3,4]
	nm		nm		nm		nm	
Carbon black	3.4±1.6	0.87±0.05	0.33±0.01	mostly m	3.5±1.6	0.85±0.06	0.34±0.01	mostly m
Pinewood soot	2±0.8	0.88±0.02	0.33±0.01	mostly m	2.4±0.7	0.86±0.04	0.33±0.01	mostly m
Beechwood soot	3.1±1.1	0.88±0.02	0.35±0.02	m & s	3.1±1.4	0.84±0.06	0.33±0.01	m & s
Wheat straw soot	2.7±0.9	0.85±0.05	0.35±0.02	mostly s	2.8±0.9	0.83±0.04	0.34±0.01	mostly s

[1] Separation distance

[2] Calculation of mean curvature and d_{sep} of graphene layers measured only on crystallites

[3,4] s - single core and m - multiple cores

The activated beechwood and wheat straw soot possessed a mixture of particles with the tightly curved graphene segments or disordered porous nanostructure, as shown in Figures 6(d)-6(f). The less ordered activated soot particles exhibited a lower packing density of graphene segments than the non-treated soot samples [55]. This probably indicates the increased macroporosity of beechwood and wheat straw soot during steam activation [56]. The pore edges of activated beechwood and wheat straw soot are irregular-shaped because the steam activation led to the collapse of pore structures. The macropore size of steam activated beechwood and wheat straw soot was not possible to determine due to the two dimensional outline of particles using TEM.

3.4. Filtration

Figure 7 shows the effects of sorbent type, duration of steam activation and initial phenol/chlorine concentrations on the water purity. The use of tire carbon black and biomass soot as sorbents decreased the phenol and chlorine concentrations almost by 20 times. The longer activation time of pinewood soot led to the complete removal of phenol from aqueous solutions, and thus, affected the water purity more than the increased activation time of tire carbon black. The phenol concentrations in filtrates using tire carbon black and pinewood soot as sorbents did not change significantly with the decreased initial phenol concentrations. The sorbent type, activation time, and initial chlorine concentration had no significant influence on the chlorine level remaining less than $1\,\mathrm{mg}$ l^{-1}. The high chlorine content ($29\,\mathrm{mg}$ l^{-1}) was determined in the filtrate using wheat straw soot as a sorbent due to the significant levels of Cl in the original material ($0.5\,\mathrm{wt.\,\%}$). The GC analysis showed that non-reacted phenol and chlorine were mostly present in filtrates, confirming the previous results of White et al. [57]. The phenol and chlorine contact time in the present study was less than $2\,\mathrm{h}$ and thus, the concentrations of chlorophenols and alkylphenols were low. The highest concentrations of 2-, 3-, and 4-chlorophenol ($4.8\,\mathrm{mg}$ l^{-1}) were measured in the extract using wheat straw soot as a sorbent.
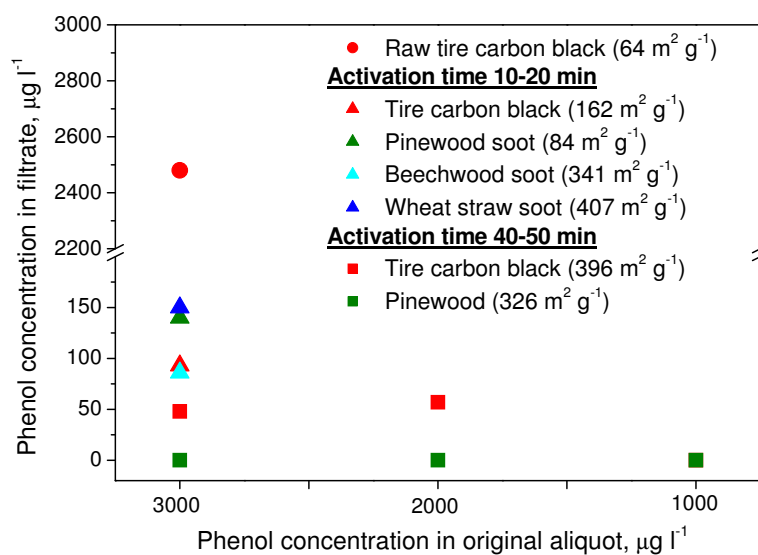
7(a): Phenol concentration
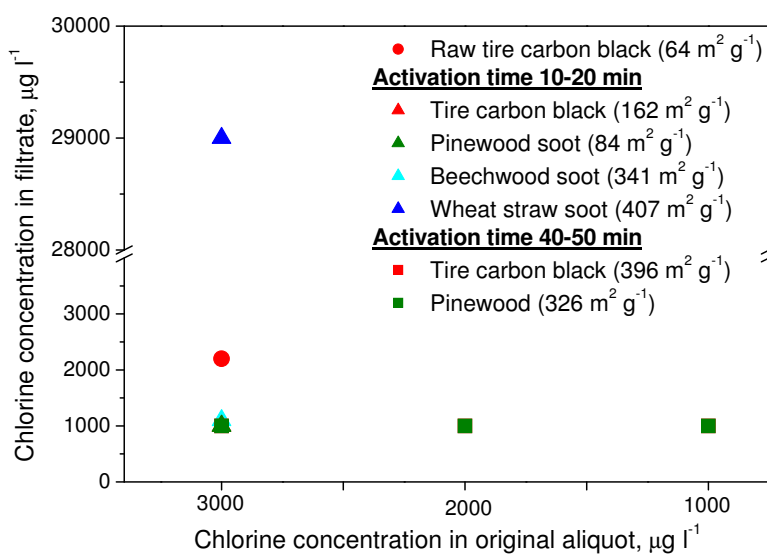
7(b): Chlorine concentration

Figure 7: Phenol and chlorine concentrations (μg l^{-1}) in filtrates using non-treated tire carbon black and activated tire carbon black, pinewood, beechwood and wheat straw soot as sorbents.

The use of non-treated tire carbon black as a sorbent removed chlorine and phenol from aqueous solution with the efficiency of 81.6 % and 73 %, whereas the activated carbon samples showed the filtration efficiency of about 95 % for both compounds.

4. Discussion

No previous work has looked into the effect of steam activation on the filter efficiency of biomass soot (and tire carbon black) and therefore it is difficult to compare the results obtained here (i.e. the influence of steam activation) with previous literature. This is the first time that steam activation experiments demonstrated significant differences in filtration efficiency of biomass soot and tire carbon black. In principle, the filtration efficiency of carbon materials can be affected by differences in particle size, soot nanostructures, ash composition, duration of steam activation, sorbent type, phenol and chlorine concentrations in wastewater. The particle size of steam activated pinewood, beechwood and wheat straw soot (46-77.7 nm) was similar to that of non-treated soot samples (44.6-78.6 nm), whereas the particle size of steam activated tire carbon black (53.7 nm) was almost twice as large as that of non-treated material (20.6 nm), as shown in Figure 4. However, the filtration efficiency of both steam activated pinewood soot and tire carbon black (95 %) was similar and at maximal conversion greater than that of steam activated beechwood and wheat straw soot samples (81.6 and 73 %). TEM analysis showed that all non-treated and steam activated soot and tire carbon black samples exhibited a nanostructure resembling carbon black based on the curvature (0.83-0.88) and separation distance (0.33-0.35 nm), as

shown in Table 3. This indicates that neither particle size nor nanostructure had a strong influence on the observed differences in filtration efficiency.

Previous work has shown that the surface area and porosity of biocarbons are prominent factors in determining their sorption properties [58, 59]. In the present study, the porosities of non-treated soot and tire carbon black samples were similar to porosities of steam activated samples with the exception being pinewood soot. These results are interesting and have not been previously looked into. The activated pinewood soot had a greater porosity with the largest total pore volume ($1.3\,\text{cm}^3\,\text{g}^{-1}$) than activated beechwood soot and tire carbon black at maximal conversion of steam activation. The beechwood soot and tire carbon black samples were less porous due to the small pore volume ranging from 0.4 to $0.6\,\text{cm}^3\,\text{g}^{-1}$. However, TEM analysis showed that activated beechwood and wheat straw soot exhibited a nanostructure with the high macroporosity, whereas pinewood soot and tire carbon black particles did not contain macropores. This indicates that the differences in macroporosity could have a significant influence on the filtration efficiency.

The activation time of biomass soot and tire carbon black was the main factor influencing the filtration efficiency. The differences in filtration efficiency of soot and tire carbon black samples activated for 10 or 40 min were significant and were attributed to feedstock differences. The long steam activation led to an increase in surface area of carbon samples and formation of new macropores in the surface due to the high diffusion rate of steam molecules into the carbon particle interior [2]. The rate of pore structure formation exceeded that of pore destruction due to the pore enlargement and

26

collapse at the earlier activation stage (10 min) and vice versa at the later steam activation stage (40 min) [60]. The surface areas of pinewood soot ($326 \, \mathrm{m^2 \, g^{-1}}$) and tire carbon black ($396 \, \mathrm{m^2 \, g^{-1}}$) were similar after 40 min of steam activation leading to similar filtration efficiencies of both sorbents. The beechwood and wheat straw soot samples obtained the highest surface area after 10 min of activation that varied from 341 to $407 \, \mathrm{m^2 \, g^{-1}}$. The mass loss of organic compounds after Soxhlet extraction of biomass soot using methanol as a solvent was in the range 0.01 to 0.02 wt. %, confirming the previous results of Trubetskaya et al. [38]. The previous results showed that the differences in nanostructure of wood and wheat straw soot were small, except for presence of single and multiple cores [44]. The potassium that is present as water-soluble alkali (i.e. KOH, KCl, K_2CO_3) contributed to the higher reactivity of ash rich beechwood and wheat straw soot in CO_2 gasification and to the formation of larger surface area of biocarbons [61, 62]. The potassium content in non-treated beechwood and wheat straw soot (1.1 wt. %) was greater than in non-treated tire carbon black (0.2 wt. %) and pinewood soot (0.07 wt. %), as shown in Table 1. Therefore, the high content of alkali metals in beechwood and wheat straw soot caused the formation of the highest surface area and large macropores during the first 10 min of steam activation leading to almost complete removal of phenol from the water. Interestingly, the presence of silicon in carbon samples had less influence on the filter performance than the alkali metals due to the similar filter efficiencies of low ash containing pinewood soot and silicon rich tire carbon black. Waste tyre carbon can be used as a precursor for the production of high quality activated carbons with the surface area ranging from 418 to $1022 \, \mathrm{m^2 \, g^{-1}}$ [29].

Previous studies showed that inorganic impurities such as sulfur and zinc retained in the activated tire carbon black during leaching emphasizing excellent properties of tire carbon black as a sorbent. In contrast, the present results also showed that the differences in initial phenol and chlorine concentrations did not affect the filter performance, probably due to the low concentrations selected in this study. The higher concentrations of phenol ($> 3000\,\mu\mathrm{g}\,\mathrm{l}^{-1}$) might affect the filter efficiency using biochar as a sorbent based on the previous studies [2, 24].

In the present study, sorbents using pinewood and tire carbon black which were activated 40 min completely removed phenol and chlorine from water, indicating a major influence of activation time on the filter efficiency. This has not been previously observed and provides key insights into the use of steam activation for enhancing the filter efficiency of soot as compared to non-treated soot materials. The carbon type affected the filter efficiency less than the presence of alkali metals which lead to the formation of greater surface area and higher amount of macropores. This shows that the filtering performance depends mostly on the ash compositional differences of sorbents using biomass soot and tire carbon black. The filtration efficiency of activated biomass soot was similarly to sugarcane bagasse based activated carbon ($> 90\,\%$) [2]. Adsorption equilibrium for phenol removal from aqueous solution on activated palm seed coat and rattan sawdust was reached within 3 h for phenol concentrations 10-60 mg l^{-1} [31, 63]. In the present study, adsorption equilibrium was reached within < 2 h. Both bio-based sorbents are more meaningsful for efficient water treatment than the non-renewable sorbents which showed a low filtration efficiency ranging between 30 and 85 % [64–67].

28

5. Conclusion

This work has demonstrated a novel method for removing toxic chemicals - phenol and chlorine - from water using steam activation. Importantly, it has been shown for the first time that steam activation of biomass soot and tire carbon black leads to significantly higher filter efficiencies compared to untreated materials for the removal of phenol and chlorine - with filter efficiencies as high as 95 % (both phenol and chlorine) for steam activated pinewood soot and tire carbon black compared to 81.6 % (chlorine) and 73 % (phenol) for the untreated material. A twenty-fold decrease in phenol and chlorine concentrations was observed using carbon black and pinewood biomass soot. Furthermore, an in-depth study correlating the filter efficiency to material properties was done; with results indicating that the presence of alkali metals and steam activation time were the key parameters affecting filter efficiencies. Increasing the steam activation time led to almost complete removal of phenol and chlorine from water using pinewood soot and tire carbon black due to the formation of greater surface area and higher amount of macropores. Therefore the work described here shows great promise for using these waste streams as cheaper alternatives for cleaning wastewater, which is of great importance for water remediation issues.

the establishment of the Center for Electron Nanoscopy in the Technical University of Denmark.

References

[1] Brown K, Water Scarcity: Forecasting the Future With Spotty Data, Science 297 (5583) (2002) 926–7.

[2] Akl MA, Dawy MB, Serage AA, Efficient Removal of Phenol from Water Samples Using Sugarcane Bagasse Based Activated Carbon, J Anal Bioanal Tech 5 (2) (2014) 1–12.

[3] Yang L, Wang Y, Song J, Zhao W, He X, Chen J, Promotion of plant growth and in situ degradation of phenol by an engineered *Pseudomonas fluorescens* strain in different contaminated environments, Soil Biol Biochem 43 (5) (2011) 915–22.

[4] Nair RJ, Sherief PM, Acute toxicity of phenol and long-term effects on food consumption and growth of juvenile rohe *Labeo rohita* under tropical condition, Abst Asian Fish Sci 10 (3) (1998) 179–87.

[5] Megharaj M, Pearson HW, Venkateswarlu K, Toxicity of phenol and three nitrophenols towards growth and metabolic activities of *Nostoc linckia*, J Env Contam Toxic 21 (4) (1991) 578–84.

[6] Carrasco-Turigas G, Villanueva CM, Goni F, Rantakokko P, Nieuwenhuijsen MJ, The Effect of Different Boiling and Filtering Devices on the Concentration of Disinfection By-Products in Tap Water, J Environ Public Health 5 (2) (2013) 1–8.

[7] Villanueva CM, Cantor KP, Cordier S, Jaakkola JJK, King WD, Lynch CF and etc., Disinfection Byproducts and Bladder Cancer A Pooled Analysis, Epidemiology 15 (2004) 357–67.

[8] Department of Health and Human Services, Public Health Statement for Phenol, U.S. Agency for Toxic Substances & Disease Registry, Atlanta, GA, https://www.atsdr.cdc.gov/phs .

[9] Spellman FR, Drinan J, Drinking Water Parameters: Microbiological. In: The Drinking Water Handbook, CRS Press LLC, 2000.

[10] Collivignarelli MC, Abba A, Alloisio G, Andrews G, Gozio E, Benigna I, Disinfection in Wastewater Treatment Plants: Evaluation of Effectiveness and Acute Toxicity Effects, Sustainability 9 (1704) (2017) 2–13.

[11] Juttner K, Galla U, Schmieder H, Electrochemical approaches to environmental problems in the process industry, Electrochim Acta 45 (2000) 2575–94.

[12] Tomaszewska M, Mozia S, Morawski W, Removal of organic matter by coagulation enhanced with adsorption on PAC, Desalination 162 (2004) 79–87.

[13] Lazarova Z, Boyadzhieva S, Treatment of phenol-containing aqueous solutions by membrane-based solvent extraction in coupled ultra filtration modules, Desalination 162 (2004) 79–87.

[14] Alderman S, Guessan A, Nyman M, Effective treatment of PAH contaminated superfund site soil with the peroxy-acid process, J Hazard Mat 163 (2007) 287–96.

[15] Sona N, Yamamoto T, Nakaiwa M, Degradation of aqueous phenol by simultaneous use of ozone with silica-gel and zeolites, Chem Eng Process 46 (2007) 513–9.

[16] Navarro AE, Cuizano NA, Lazo JC, Sun-Kou MR, Llanos BP, Comparative study of the removal of phenolic compounds by biological and non-biological adsorbents, J Hazard Mater 164 (2009) 1439–46.

[17] Lazo-Cannata JC, Nieto-Marquez A, Jacoby A, Paredes-Doig AL, Romero A, Adsorption of phenol and nitrophenols by carbon nanospheres: Effect of pH and ionic strength, Sep Purific Tech 80 (2011) 217–24.

[18] Ravindran V, Stevens MR, Badriyha BN, Pirbazari M, Modeling the sorption of toxic metals on chelant-impregnated adsorbent, AIChE J 45 (1999) 1135–46.

[19] Toles CA, Marshall WE, Copper ion removal by almond shell carbons and commercial carbons: batch and column studies, Sep Sci Tech 37 (2002) 2369–83.

[20] Lehmann CMB, Rostam-Abadi M, Rood MJ, Sun J, Reprocessing and Reuse of Waste Tire Rubber to Solve Air-Quality Related Problems, Energy Fuels 12 (1998) 1095–9.

[21] Alhamed YA, Phenol removal using granular activated carbon from date stones, Bulg Chem Comm 41 (2008) 26–35.

[22] Chakraborty A, Deva D, Sharma A, Verma N, Adsorbents based on carbon microfibers and carbon nanofibers for the removal of phenol and lead from water, J Colloid Interface Sci 359 (1) (2011) 228–39.

[23] Sarkar M, Acharya PK, Use of fly ash for the removal of phenol and its analogues from contaminated water, Waste Manage 26 (6) (2006) 559–70.

[24] Thompson KA, Shimabuku KK, Kearns JP, Knappe DRU, Summers RS, Cook SM, Environmental Comparison of Biochar and Activated Carbon for Tertiary Wastewater Treatment, Environ Sci Tech 50 (2016) 11253–62.

[25] Kennedy LJ, Vijaya JJ, Sekaran G, Effect of two-stage process on the preparation and characterization of porous carbon composite from rice husk by phosphoric acid activation, Ind Eng Chem Res 43 (2004) 1832–8.

[26] Berezkin VI, Viktorovskii IV, Golubev LV, Petrova VN, Khoroshko LO, A comparative study of the sorption capacity of activated charcoal, soot, and fullerenes for organochlorine compounds, Tech Phy Letters 28 (11) (2002) 885–8.

[27] Teng H, Lin YC, Hsu LY, Production of Activated Carbons from Pyrolysis of Waste Tires Impregnated with Potassium Hydroxide, J Air Waste Manage Assoc 50 (2000) 1940–6.

[28] Helleur R, Popovic N, Ikura BY, Stanciulescu M, Liu D, Characterization and potential applications of pyrolytic char from ablative pyrolysis of used tires, J Anal Appl Pyrolysis 58 (2001) 813–24.

[29] Miguel GS, Fowler GD, Sollars CJ, The leaching of inorganic species from activated carbons produced from waste tyre rubber, Water Res 36 (2002) 1939–46.

[30] El-Hendawy A, Samra SE, Girgis BS, Adsorption characteristics of activated carbons obtained from corncobs, Coll Surf A: Phys Eng Aspects 180 (3) (2001) 209–21.

[31] Rengaraj S, Moon SH, Sivabalan R, Arabindoo B, Murugesan V, Agricultural solid waste for the removal of organics: adsorption of phenol from water and wastewater by palm seed coat activated carbon, Waste Manage 22 (2002) 543–8.

[32] Sun L, Wang C, Zhou Y, Zhang X, Qiu J, KOH-activated depleted fullerene soot for electrochemical double-layer capacitors, J Appl Electrochem 44 (2014) 309–16.

[33] Wu FC, Tseng RL, Juang RS, Comparisons of porous and adsorption properties of carbons activated by steam and KOH, J Colloid Interface Sci 283 (1) (2005) 49–56.

[34] Ariyadejwanicha P, Tanthapanichakoona W, Nakagawab K, Mukaib SR, Tamon H, Preparation and characterization of mesoporous activated carbon from waste tires, Carbon 41 (2003) 157–64.

[35] Miguel GS, Fowler GD, Sollars CJ, A study of the characteristics of activated carbons produced by steam and carbon dioxide activation of waste tyre rubber, Carbon 41 (2003) 1009–16.

[36] Mui E, Ko DCK, McKay G, Production of active carbons from waste tyres - a review, Carbon 42 (14) (2004) 2789–2805.

[37] Umeki K, Häggström G, Bach-Oller A, Kirtania K, Furusjö E, Reduction of Tar and Soot Formation from Entrained-Flow Gasification of Woody Biomass by Alkali Impregnation, Energy Fuels 31 (2017) 5104–10.

[38] Trubetskaya A, Brown A, Tompsett GA, Timko MT, Kling J, Broström M, Larsen Andersen M, Umeki K, Characterization and reactivity of soot from fast pyrolysis of lignocellulosic compounds and monolignols, Appl Energy 212 (2018) 1489–500.

[39] Rasband WS, Image J, U.S. National Institutes of Health: Bethesda, MD, http://imagej.nih.gov/ij .

[40] Cenker E, Bruneaux G, Dreier T, Schulz C, Determination of small soot particles in the presence of large ones from time-resolved laser-induced incandescence, Appl Phys B 118 (2015) 169–83.

[41] Landers J, Gor GY, Neimark AV, Density functional theory methods for characterization of porous materials, Coll Surf A: Physicochem Eng Aspects 437 (2013) 3–32.

[42] Thommes M, Kaneko K, Neimark AV, Olivier JP, Rodriguez-Reinoso F, Rouquerol J and etc., Physisorption of gases, with special reference to the evaluation of surface area and pore size distribution (IUPAC Technical Report), Pure Appl Chem 87 (2015) 1051–69.

[43] Vohler O, Reiser PL, Martina R, Overhoff D, New Forms of Carbon, Angew Chemie 9 (6) (1970) 414–25.

[44] Trubetskaya A, Jensen PA, Jensen AD, Garcia Llamas AD, Umeki K, Gardini D and etc., Effects of several types of biomass fuels on the yield, nanostructure and reactivity of soot from fast pyrolysis at high temperatures, Appl Energy 171 (2016) 468–82.

[45] Schröder E, Thomauske K, Oechsler B, Herberger S, Activated Carbon from Waste Biomass. In: Progress in Biomass and Bioenergy Production, Intechopen, 2011.

[46] Jauregui O, Galceran MT, Chapter 6 Phenols. In: Handbook of Analytical Separations, ScienceDirect, 2001.

[47] Pagketanang T, Artnaseaw A, Wongwicha P, Thabuot M, Microporous Activated Carbon from KOH-Activation of Rubber Seed-Shells for Application in Capacitor Electrode, Energy Procedia 79 (2015) 651–6.

[48] Chakrabarty RK, Moosmüller H, Garro MA, Arnott WP, Walker J, Susott RA et al., Emissions from the laboratory combustion of wildland fuels: Particle morphology and size, J Geophys Research 111 (D7) (2006) 1–16.

[49] Sachdeva K, Attri AK, Morphological characterization of carbonaceous aggregates in soot and free fall aerosol samples, Atmos Environ 42 (5) (2008) 1025–34.

[50] Liati A, Eggenschwiler PD, Schreiber D, Zelenay V, Ammann M, Variations in diesel soot reactivity along the exhaust after-treatment system, based on the morphology and nanostructure of primary soot particles, Combust Flame 160 (3) (2013) 671–81.

[51] Lee KO, Cole R, Sekar R, Kang J, Bae C, Zhu J, Detailed Characterization of Morphology and Dimensions of Diesel Particulates via Thermophoretic Sampling, Sae Tech Papers (2001) 1–10.

[52] Zeng Q, Wang DW, Wu KH, Li Y, de Codoi FC, Gentle IR, Synergy of nanoconfinement and surface oxygen in recrystallization of sulfur melt in carbon nanocapsules and the related Li-S cathode properties, J Mater Chem A 2 (2014) 6439–47.

[53] Müller JO, Su DS, Wild U, Schlögl R, Bulk and surface structural investigations of diesel engine soot and carbon black, Phys Chem Chem Phys 9 (2007) 4018–25.

[54] Sui ZY, Meng QH, Li JT, Zhu JH, Cui Y, Han BH, High surface area porous carbons produced by steam activation of graphene aerogels, J Mat Chem A 2 (2014) 9891–9.

[55] Harris PJF, Liu Z, Suenaga K, Imaging the atomic structure of activated carbon, J Phys Condens Matter 20 (2008) 1–5.

[56] Lin W, Xu B, Liu L, Hierarchical porous carbon prepared by NaOH activation of nano-$CaCO_3$ templated carbon for high rate supercapacitors, New J Chem 38 (2014) 5509–14.

[57] White JT, Bursztynsky TA, Crane JD, Jones RH, Treating Wood Preserving Plant Wastewater. Cincinnatio (OH): Industrial Environmental Reseaerch Laboratory; 1976 September Report No. EPA-600-276231. Contract No.: 12100-HIG .

[58] Akl MA, Atta A, Youssef AM, Ibraheim MA, The Utility of Novel Superabsorbent Core Shell Magnetic Nanocomposites for Efficient Removal of Basic Dyes from Aqueous Solutions, J Chrom Separation Tech 4 (5) (2013) 1–9.

[59] Salame II, Bagreev A, Bandosz TJ, Revising the effect of surface chemistry on adsorption of water on activated carbons, J Phy Chem B 103 (1999) 3877–84.

[60] Santorun-Shalaby C, Ucak-Astarlioglu MG, Artok L, Sarici C, Preparation and characterization of activated carbons by one-step steam pyrolysis/activation from apricot stones, Micropor Mesopor Mater 88 (2006) 126–34.

[61] Trubetskaya A, Hofmann Larsen F, Shchukarev A, Stå hl K, Umeki K, Potassium and soot interaction in fast biomass pyrolysis at high temperatures, Fuel 225 (2018) 89–94.

[62] Hagemann N, Spokas K, Schmidt HP, Kä gi R, Bö hler MA, Bucheli TD, Activated Carbon, Biochar and Charcoal: Linkages and Synergies across Pyrogenic Carbon's ABCs, Water 10 (182) (2018) 1–19.

[63] Hameed BH, Rahman AA, Removal of phenol from aqueous solutions by adsorption onto activated carbon prepared from biomass material, J Hazar Mat 160 (2008) 576–81.

[64] Matthes W, Kahr G, Sorption of organic compounds by Al and Zr-hydroxy-intercalated and pillared bentonite, Clays clay minerals 48 (2000) 593–602.

[65] Srihari V, Das A, Adsorption of phenol from aqueous media by an agrowaste (Hemidesmus indicus) based activated carbon, Appl Ecol Environ Res 7 (2009) 13–23.

[66] Maarof HI, Hameed BH, Ahmad AL, Adsorption isotherms for phenol onto activated carbon, ASEAN J Chem Eng 4 (2004) 70–6.

[67] Haque E, Khan NA, Talapaneni SN, Vinu A, JeGal JG, Jhung SH, Adsorption of Phenol on Mesoporous Carbon CMK-3: Effect of Textual Properties, Bull Kor Chem Soc 31 (6) (2010) 1638–42.